(a)

Joint	Phase 1 Direction	Phase 1 Mode	Phase 2 Direction	Phase 2 Mode
Hip	Flexion	Active	Extension	Active
Knee	Flexion ↓ Extension	Free	Flexion ↓ Extension	Passive

(b)

Joint	Phase 1 Direction	Phase 1 Mode	Phase 2 Direction	Phase 2 Mode	Phase 3 Direction	Phase 3 Mode	Phase 4 Direction	Phase 4 Mode
Hip	—	Static	Flexion	Active	Extension	Active	—	Static
Knee	—	Static	Extension	Active	Extension	Active	—	Static

(c)

Joint	Phase 1 Direction	Phase 1 Mode	Phase 2 Direction	Phase 2 Mode	Phase 3 Direction	Phase 3 Mode
Hip	Extension	Active	Extension	Free	Extension	Active
Knee	Flexion	Free	Extension	Free	Extension	Active

Figure 6. Joint part detection and mode of dynamic motion in each Phase: (a) walking, (b) standing up and (c) going up stairs.

are performed reacting to the FRF. Therefore, it would be effective to determine Phase-shift timing from the FRF.

3.3.1. Walking. We focus on the condition of the left FRF for Phase-shift timing of the right leg. During walking the right leg swings (Phase 1 starts) when the rear part of the left foot contacts with the ground surface (Fig. 5a). At this time, we should be able to detect the FRF at the rear part of left foot and this detection can be used as an indication for the start of Phase 1. On the other hand, Phase 2 starts when the right foot contacts with the ground surface while the ground contact part of the left foot shifts to the front. As the result we should be able to detect the increasing in FRF at the front part of the left foot and use it as the indicator for the start of Phase 2. Based on these characteristics of the FRF, we set thresholds for FRF at the front and rear part of the left foot (V_{lf}, V_{lr}) which indicate the ground contact. If the FRF value at the front part of the left foot (f_{lf}) exceeds the threshold of the FRF at the front part of the left foot (V_{lf}), Phase 1 shifts to Phase 2. Subsequently, if the FRF value at the rear part of the left foot (f_{lr}) exceeds the threshold of the FRF at the rear part of the left foot (V_{lr}), Phase 2 shifts to Phase 1. We use the same method to determine the Phase-shift timing of the left leg based on the FRF of the right foot. The flow chart of the Phase Sequence in walking power assist for the right leg is shown in Fig. 7a.

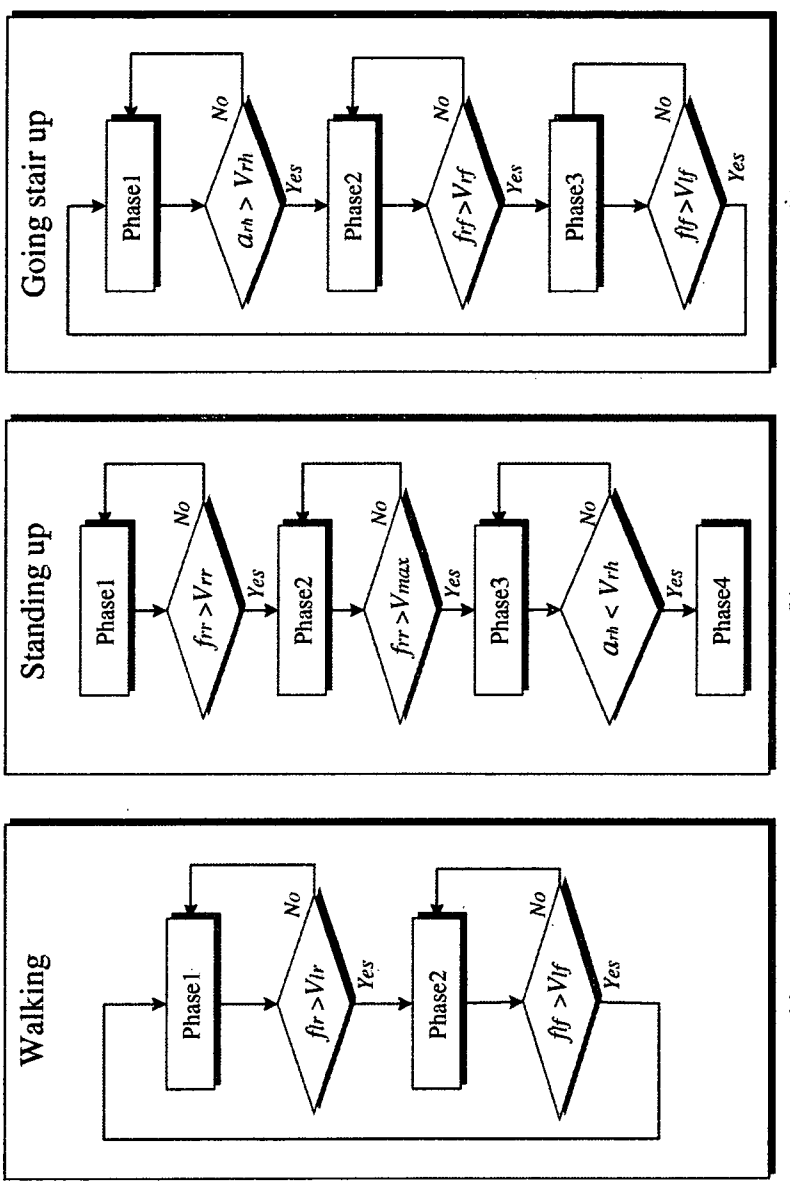

Figure 7. Flow charts for Phase Sequence: (a) walking, (b) standing up and (c) going up stairs.

3.3.2. Standing up. We use the condition of the FRF at the rear part of the right foot (f_{rr}) and the right hip joint (a_{rh}) in order to determine Phase-shift timing for standing up motion. As shown in Fig. 5b, when the upper body is slightly bent forward from the sitting position (Phase 2 starts), f_{rr} is detected. At this time, this detection can be used as an indication for the start of Phase 2. Phase 3 starts when f_{rr} exceeds approximately 80% of the maximum value. The hip and knee joints are extended in Phase 3. Finally, the standing up motion settles down in Phase 4 as the standing position. Based on these characteristics of FRF, we set thresholds for FRF at the rear of the right foot which indicate the condition for the shifts to Phase 2 and Phase 3, respectively. If f_{rr} exceeds the threshold (V_{rr}), Phase 1 shifts to Phase 2. Subsequently, if f_{rr} attains 80% of the maximum value (V_{max}) which is obtained from previous data of motion without the power assistance, Phase 2 shifts to Phase 3. Finally, if the right hip joint angle (a_{rh}) attains the predefined threshold (V_{rh}), Phase 3 is changed into Phase 4. The flow chart of the Phase Sequence in standing up power assist is shown in Fig. 7b.

3.3.3. Going up stairs. We use the condition of FRF at the front part of both feet and the right hip joint for the determination of Phase-shift timing of the right leg. As shown in Fig. 5c, during the going up stairs motion, the right leg is lifted up (Phase 1 starts) when the front part of the left foot contacts with the stair surface. At this time, we should be able to detect the FRF at the front part of the left foot and this detection can be used as an indication for the start of Phase 1. Phase 2 starts when the right hip joint angle attains the maximum value. Phase 3 starts when the right foot contacts with the ground surface. As a result we should be able to detect FRF at the front part of the right foot and use it as the indicator for the start of Phase 3. Based on these characteristics of the FRF and joint angle, we set thresholds for the FRF at the front part of the left and right foot (V_{lf}, V_{rf}) and the right hip joint angle (V_{rh}). If the FRF value at the front part of the left foot (f_{lf}) exceeds the predefined threshold (V_{lf}), Phase 1 starts. Subsequently, if the hip joint angle value (a_{rh}) attains the threshold (V_{rh}), Phase 1 shifts to Phase 2. If the FRF value at the front part of the right foot (f_{rf}) exceeds the predefined threshold (V_{rf}), Phase 2 shifts to Phase 3. We use the same method to determine the Phase-shift timing of the left leg based on the FRF at front part of both feet and the left hip angle. The flow chart of the Phase Sequence in going up stairs power assist is shown in Fig. 7c.

4. EXPERIMENTAL VERIFICATION

4.1. Method

The power assist experiments described in this section were performed with the Phase Sequence control defined in Section 3. In these experiments, power assist was performed for the active mode in each Phase by using HAL-3. The assist torque in each active mode was adjusted according to each Phase on the basis of the wearer's

feedback suggestions. The assist torque pattern of each active mode is generated as a rectangular wave. Each threshold of the FRF for the Phase shift is determined based on the exoskeleton performance without any power assist. On the other hand, we set the threshold angles depending on the height of the chair or the stair used in this experiment. There is certain range for the thresholds necessary to transit Phases successfully. We determined the thresholds so that they could fall within this range. If the height of the chair or the stair was slightly different, Phases were successfully transited by using the thresholds.

It is considered that the assisted muscle's activation level during adequate power assist motion is reduced compared to the activation level of the motion without the power assist. However, the muscle's activation level during power assist motion with a time-delay of Phase switching is increased compared to that of the motion without the power assit. The muscle's activation level during each Phase is defined using the average myoelectric signal:

$$A = \frac{1}{T_p} \int_{t_s}^{t_s+T_p} E(t)\,dt, \tag{1}$$

where $E(t)$ is the calibrated myoelectric signal and is a quatitative value related to the joint torque generated during the isometric contraction of the muscle; t_s and T_p represent the start time and the period of each Phase. The effect of the power assist was evaluated by comparison between the muscle's activation level with and without the power assist. The wearer was a normal 28-year-old male. Assist torque values were practically measured from the electric current consumed by the drive motors.

4.2. Experimental results

4.2.1. Walking. Thresholds of the FRF at the front and rear part of each foot for Phase shift were set as 640 and 180 N, respectively. The assist torques of the hip joint on the active modes on Phases 1 and 2 were 8 N, respectively. Figure 8a shows the joint angles, myoelectric signals and assist torques for the hip and knee joint, and the FRF in the front and rear parts of both feet during walking with power assist. The relation between the hip joint angle and the assist torque indicates smooth Phase shift. Figure 9a shows the averages of the muscle's activation levels at the hip flexor in Phase 1, and the hip extensor in Phase 2, during 10 steps of the right leg with and without power assist, respectively. It is obvious that the muscle's activation levels with the power assist are reduced compare to those without power assist.

4.2.2. Standing up. Thresholds for shifting to Phases 2, 3 and 4 were set as 60 N, 350 N and 0.1 rad, respectively. The assist torques of the hip and knee joints on the active modes of Phases 1 and 2 were 24 N, respectively. Figure 8b shows the joint angles, myoelectric signals and assist torques for the hip and knee joint, and the FRF at the rear parts of the right foot during standing up with power assist. The

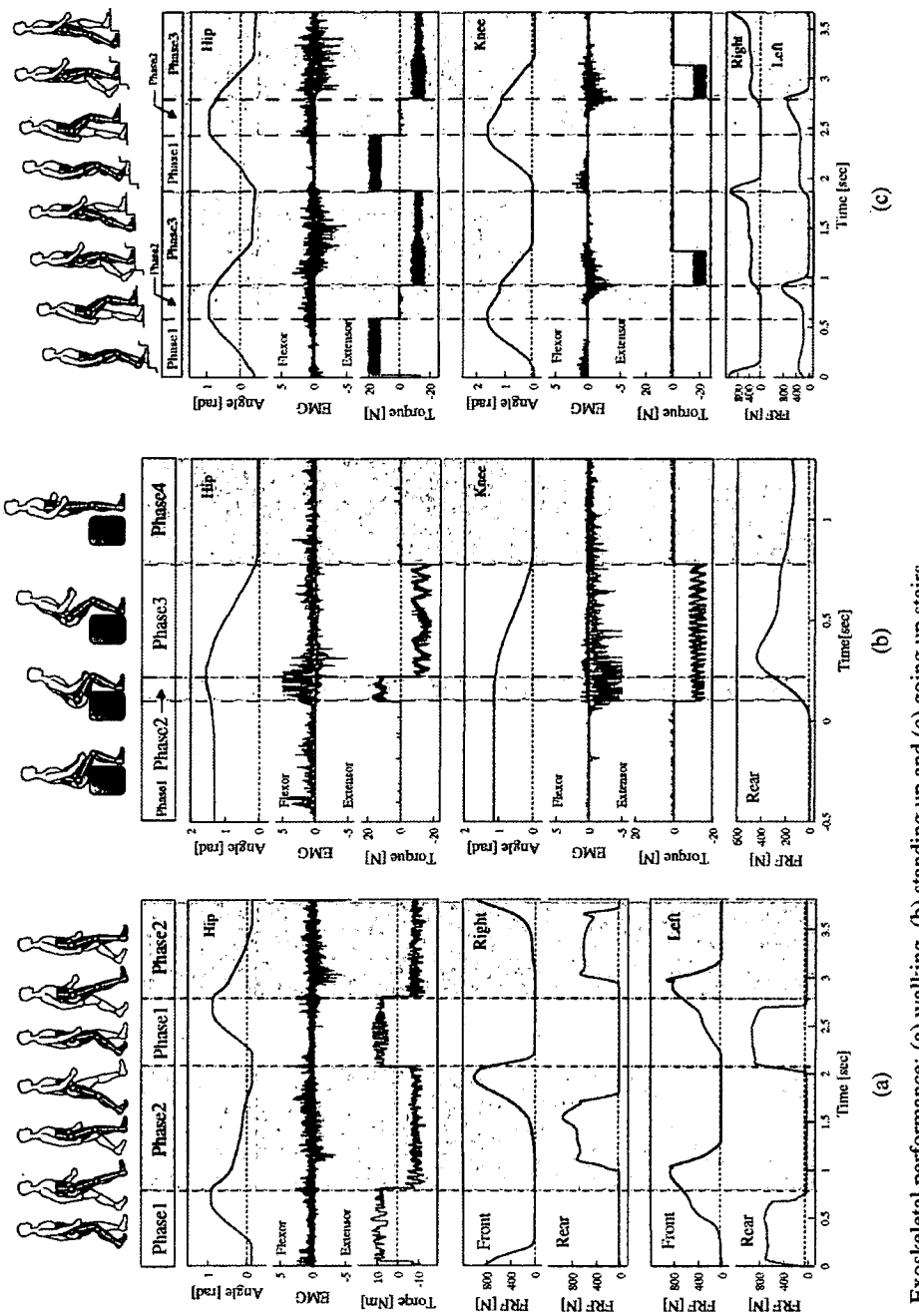

Figure 8. Exoskeletal performance: (a) walking, (b) standing up and (c) going up stairs.

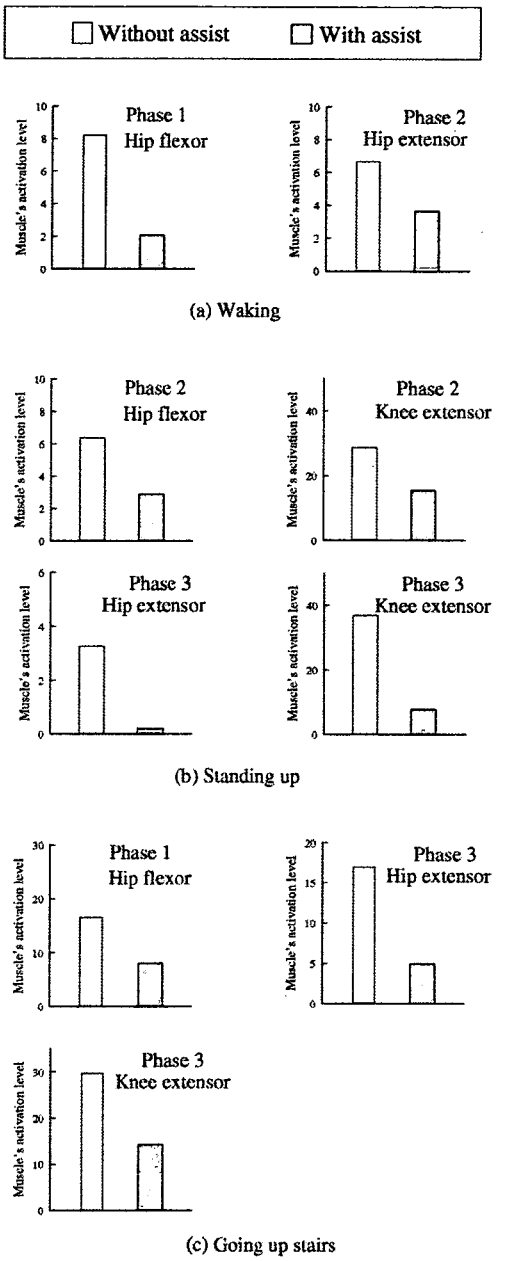

Figure 9. Comparison of the muscle activation levels for each Phase with and without the power assist.

behavior of the hip and knee joint angles is similar to that without the power assist (Fig. 5b). Figure 9b shows the averages of the muscle's activation levels at the hip flexor and the knee extensor in Phase 2, and the hip and knee extensor in Phase 3, during standing up with and without power assist 10 times, respectively. It is clear

that the muscle's activation levels with the power assist are reduced relative to those without power assist.

4.2.3. Going up stairs. Thresholds for shifting to Phases 1, 2 and 3 were set as 160 N, 0.9 rad and 160 N, respectively. The assist torques of the hip joint on the active modes of Phase 1 were 16 N. Those of the hip and knee joints on Phase 3 were 12 and 20 N, respectively. Figure 8c shows the joint angles, myoelectric signals and assist torques for the hip and knee joint, and the FRF at the front part of both feet during going up stairs with power assist. It is clear that each Phase is shifted by using the predefined thresholds for the FRF at the front part of both of the feet and the hip angle. Figure 9c shows the averages and standard deviations of the muscle's activation levels at the hip flexor in Phase 1, and the hip and knee extensor in Phase 3, during 10 steps of the right leg with and without power assist, respectively. It is clear that the muscle's activation levels with the power assist are reduced relative to those without power assist.

4.3. Discussion

For each task, the hip and knee angle joints with power assist as shown in Fig. 8 were similar to those of motions without power assist as shown in Fig. 5. It is obvious that the Phases for each task were successfully transited and the tasks were realized. The activation levels of the muscles assisted in active mode were significantly reduced relative to the activation levels without the assistance (Fig. 9). This fact indicates that the autonomous motions generated by an exoskeleton robot effectively move the human's leg without any time-delay in Phase swiching. Therefore, we confirmed that the Phase Sequence method based on the modes of muscle activity is effective as an assist method by using autonomous motion of the exoskeleton robot HAL-3.

In the case of walking, we performed the assist including the active mode for the hip joint necessary to move forward and confirmed the feasibility. The assist including the passive and free mode for the knee joint was not performed. Further research should focus on adapting the power assist for the passive mode and the free mode by using the impedance control method [12].

The assist torque in each Phase was determined based on feedback suggestions from the wearer. We estimated the effectiveness of the assist by using the muscle's activation level. The reduction of the muscle's activation level differed according to the Phases. We have developed a method to adjust the assist torque on the basis of the muscle's activation level as a controlled variable [13]. The controller adjusting the assist torque in each Phase will provide more comfortable power assist for the wearer. Moreover, it is important to secure the safety of users of HAL. We have to note the risk of falling over caused by tripping, etc. We have studied the autonomous posture control method to prevent falling in parallel with the power assist methods.

In the near future, we will develop an autonomous motion assist method that applies the posture controller. Considering individual variations, we will use this method depending on the users of the HAL. In the case of a normal user, the

thresholds for Phase-shift timing are determined based on the motion analysis data of individual users of the HAL. It is not necessary to measure the basic EMG signal because the FRF value and joint angle are used as indications for Phase-shift timing. The thresholds for the Phase-shift timing are determined according to individual users. However, it is convenient to use the EMG signal in order to analyze the muscle's condition during different motions or estimate the effectiveness of the assist. In the case of a handicapped user, the motion assist should be performed according to the standard motion. The standard motion has to be statistically determined based on motion analysis data of a number of normal persons. We plan to report on this issue in the near future.

5. CONCLUSIONS

In this research we proposed an assist method on the basis of autonomous motion of an exoskeleton robot. In order to perform tasks (walking, standing up and going up stairs) autonomically, we used Phase Sequence control, which generates a task by transiting some simple basic motions called Phases. Tasks were divided into some Phases during the tasks performed by a normal person. The joint moving modes were categorized into active, passive and free modes based on the characteristic of the muscle force conditions. The autonomous motion which HAL generates in each Phase were designed according to one of the categorized modes. FRFs and joint angles were adopted to transit each Phase. Power assist experiments were performed by using autonomous motion with a focus on the active mode. The experimental results showed that the muscle activation levels in each Phase were reduced. With this, we confirmed the effectiveness of the proposed assist method.

REFERENCES

1. H. Kazerooni and S. L. Mahoney, Dynamics and control or robotic systems worn by humans, *J. Dynamic Syst. Meas. Control* **113**, 379–387 (1991).
2. H. Kazerooni and S. L. Mahoney, Human extenders, *J. Dynamic Syst. Meas. Control* **115**, 281–290 (1993).
3. Y. Hayashibara, K. Tanie and H. Arai, Design of a power assisted system with consideration of actuator's maximum torque, in: *Proc. IEEE Int. Workshop on Robot and Human Communication*, Tokyo, pp. 397–384 (1995).
4. J. Rosen *et al.*, A myosignal-based powered exoskeleton system, *IEEE Trans. Syst. Man Cybernet. A* **31**, 210–222 (2001).
5. T. Nakai, S. Lee, H. Kawamoto and Y. Sankai, Development of power assistive leg for walking aid using EMG and linux, in: *Proc. 2nd Asian Symp. on Industrial Automation and Robotics*, Bangkok, pp. 295–299 (2001).
6. K. Kasaoka and Y. Sankai, Predictive control estimating operator's intention for stepping-up motion, in: *Proc. Int. Workshop on Intelligent Robots and Systems*, Maui, HI, pp. 1578–1583 (2001).
7. S. Lee and Y. Sankai, Power asssit control for walking aid by HAL based on phase sequence and EMG, in: *Proc. Int. Conf. on Control, Automation and System*, Cheju, pp. 353–356 (2001).

8. H. Kawamoto and Y. Sankai, EMG-based hybrid assistive leg for walking aid using feedforward controller, in: *Proc. Int. Conf. on Control, Automation and System*, Cheju, pp. 190–193 (2001).
9. H. Imai, M. Nozawa, Y. Kawamura and Y. Sankai, Human motion oriented control method for humanoid robot, in: *Proc. Int. Workshop on Robot and Human Interactive Communication*, Berlin, pp. 221–226 (2002).
10. Y. Kawamura and Y. Sankai, Humanoid control method based on human knack for human care service, in: *Proc. Int. Conf. on System, Man and Cybenetics*, Hammamet, TP1B4 (CD-ROM) (2002).
11. M. Kumagai and T. Emura, A method for controlling robots using common Linux, in: *Proc. 17th Ann. Conf. of the Robotics Society of Japan*, Hiratsuka, pp. 847–848 (1999).
12. S. Lee and Y. Sankai, Power assist control for walking aid with HAL-3 based on EMG and impedance adjustment around knee joint, in: *Proc. Int. Conf. of Intelligent Robots and Systems*, Hammamet, TP1B3 (CD-ROM) (2002).
13. H. Kawamoto and Y. Sankai, Power assist method for HAL-3 using EMG-based feedback controller, in: *Proc. Int. Conf. on System, Man and Cybenetics*, Washington, DC, pp. 1648–1653 (2003).

ABOUT THE AUTHORS

Hiroaki Kawamoto received the BE, ME and PhD degrees from the University of Tsukuba, Japan in 1998, 2000 and 2004, respectively. Currently he is a Research Assistant at the University of Tsukuba Venture Business Laboratory. His research interests include biomechanics, biorobotics and the human–machine interface, especially exoskeletal robots. He is a member of the Robotics Society of Japan and Japan Society of Mechanical Engineers.

Yoshiyuki Sankai received the PhD degree in engineering from the University of Tsukuba, Japan in 1987. He was a JSPS research fellow, Assistant Professor, Associate Professor and Professor of Institute of Systems and Engineering in the University of Tsukuba, and a Visiting Professor of Baylor College of Medicine in USA. Currently, he is a professor and director of the prioritized research area 'New Robotics Frontier: Cybernics', Graduate School of System and Information Engineering in University of Tsukuba, Japan. His research interests include Robot Suit HAL (Hybrid Assistive Limb), the next generation artificial heart, humanoid Control, Bio-Medical Science, Network Medicine as related fields of Cybernics. He received a Grant of the Japanese Society for Artificial Organs (JSAO), Awards from American Society for Artificial Organs, International Society for Artificial Organs, International Society for Rotary Blood Pump with his students and so on. He was/is a president of Japan Society of Embolus Detection and Treatment, a chair of *International Journal of the Robotics Society of Japan*, a member of Awards Committee in the Robotics Society of Japan and Japan Society of Mechanical Engineers, an executive editor of Vascular Lab., an executive board member of Robotics Society of Japan, a founder and a chairman of CYBERDYNE Inc.

Advanced Robotics, Vol. 19, No. 7, pp. 773–795 (2005)

Also available online - www.vsppub.com

Full paper

Virtual impedance adjustment in unconstrained motion for an exoskeletal robot assisting the lower limb

SUWOONG LEE * and YOSHIYUKI SANKAI

Graduate School of Systems and Information Engineering, University of Tsukuba, 1-1-1 Tennodai, Tsukuba, Ibaraki 305-8573, Japan

Received 11 May 2004; accepted 12 August 2004

Abstract—The objective of this paper is to establish the criteria for adjusting the virtual impedance of an exoskeletal robot for the lower limb in order to minimize the operator's physical stress in unconstrained motion. The exoskeletal robot HAL (Hybrid Assistive Limb)-3 which we developed for assisting the motor function of the lower limb was used for experiments in this research. To accomplish the objective (i) the physical parameters around the joint of HAL-3 were identified and (ii) the relationships between the virtual impedance values and the physical stress of operators were examined through experiments for swinging motions of the lower leg. The physical stress was evaluated with myoelectricity, the musculoskeletal moment of the operator and the operator's feelings during the experimental motion. As a result, we found that the physical stress tended to decline with the decrease of virtual inertia and virtual Coulomb friction, and to increase slightly with the decrease of virtual gravitational moment. The decrease of virtual viscous friction made the physical stress increase gradually after it declined to a trough during the positive virtual viscous friction. Based on the results, we could establish the criteria for adjusting the virtual impedance for minimizing the operator's physical stress in unconstrained motion.

Keywords: Assist; virtual impedance; physical stress; parameter identification; unconstrained motion.

1. INTRODUCTION

Exoskeletal robot suits aimed at supporting the works of labor or the movements of aged persons have the ideal form to assist a human's motion, and they are expected to be used in many fields such as labor-intensive industries, welfare and medicine. In particular, it is likely that exoskeletal robots for assisting the motor function of the lower limb will be very useful for supporting a human's locomotion in the work area or living space [1–3].

*To whom correspondence should be addressed. E-mail: lee@golem.kz.tsukuba.ac.jp

The states of the leg in some motions, such as walking or standing up, can be divided into two types, depending on whether the foot contacts the floor or not, as shown in Fig. 1. The former is defined as constrained motion and the latter as unconstrained motion in this paper. To realize effective assistance of the lower limb with an exoskeletal robot, it is required to not merely amplify the moment around the human's joints of the lower limb, but also to adjust the virtual impedance of the robot suitable for various motion types. Focusing attention on the adjustment of virtual impedance in unconstrained motion, since a human can swing the lower limb with a minimum amount of moment by using inertia and gravitational moment [4], the virtual impedance of exoskeletal robots needs to be adjusted properly so that the physical stress is minimized. A number of studies related to exoskeletal robots for the lower limb have been performed [1–3]; however, so far the study of the impedance adjustment has been superficial. Researchers who studied impedance adjustment of robots assisting a human's work have reported tracking control properties of human–robot systems analyzed for different values of the robot impedance [5] and a method for adjusting the impedance in positioning control of robot which assists the worker's operation [6]. The impedance properties of humans and robots in positioning the upper limb along the desired point or trajectory were discussed. However, a human's motion includes non-voluntary movement (like an unconstrained leg in walking) as well as voluntary movement. Therefore, in order to assist the motion of the lower limb with an exoskeletal robot, the properties in unconstrained motion should be considered.

The purpose of this paper is to establish the criteria for adjusting the virtual impedance of an exoskeletal robot for the lower limb in order to minimize the operator's physical stress in unconstrained motion. Section 2 introduces the exoskeletal robot. HAL (Hybrid Assistive Limb)-3 which was used in the experiments. Section 3 explains the parameter identification around the joint of HAL-3, the exper-

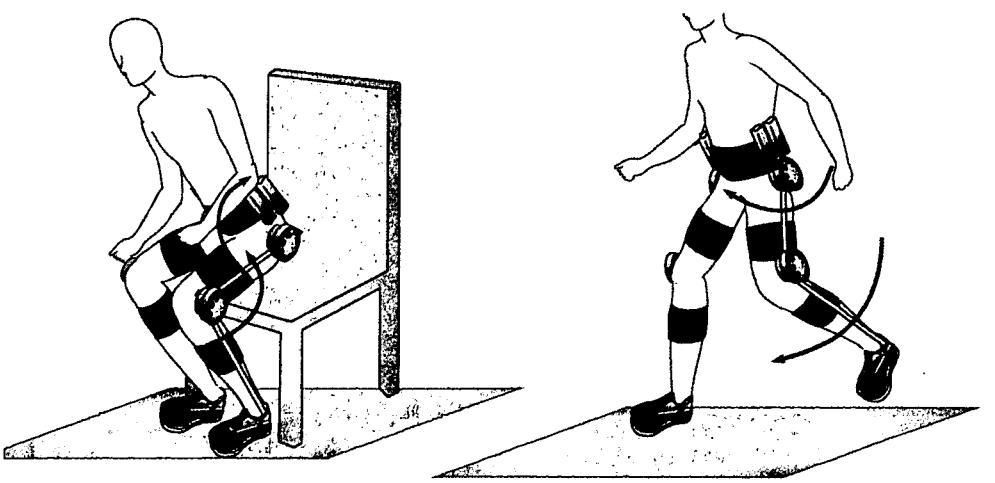

Figure 1. Constrained motion (left) and unconstrained motion (right) of the lower limb.

imental setups and the evaluation methods for the experimental results. Section 4 examines and evaluates the relationships between the virtual impedance values and the physical stress of the operators through experiments for unconstrained motions of the lower leg. Section 5 discusses the experimental results.

2. HAL-3

2.1. Hardware configuration of HAL-3

Figures 2 and 3 show the hardware configuration and the structure of the exoskeleton-type power assist system HAL-3 used in the experiments. It consists of a three-link, two-joint mechanism corresponding to the human lower limb. The joints of the exoskeleton are powered by actuators composed of DC servo motors and gears, and controlled in torque control mode according to an operational signal from a control computer. Mechanical constraints attached to joints keep the joint angle of the exoskeleton within human anthropometric boundaries. Potentiometers are attached to the center of the exoskeletal joint axes so as to measure the angle of joints and force sensors are mounted at the exoskeletal frame to measure the force applied by the operator to the exoskeleton of HAL-3. Myoelectric electrodes are attached on the operator's skin for measuring the myoelectric signal of the flexor and extensor muscles of the joint. In this paper, experiments focused on the motion

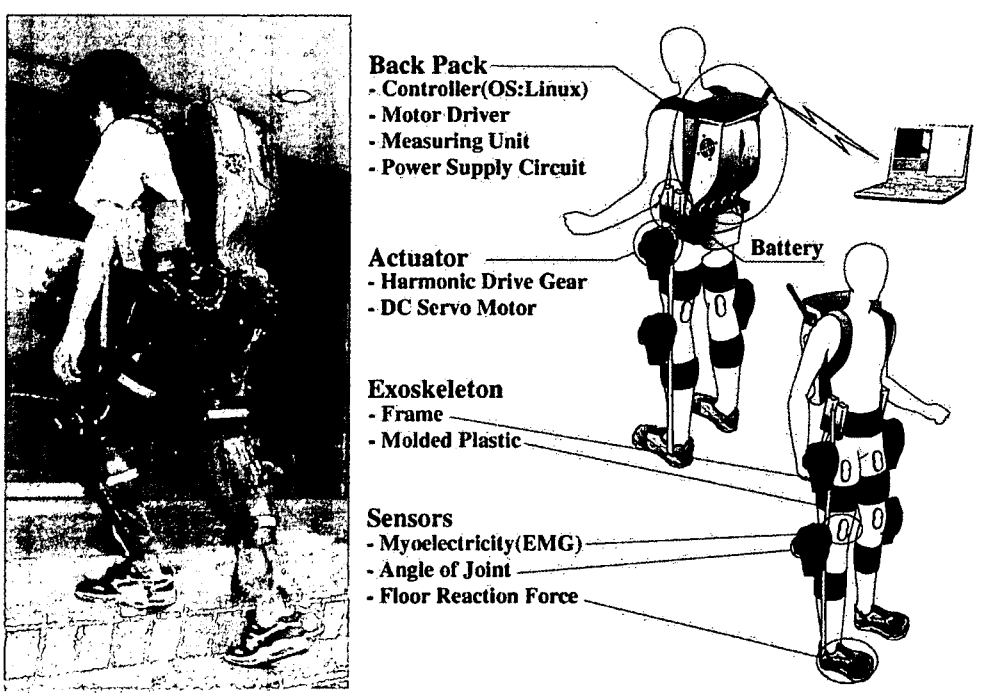

Figure 2. HAL-3.

Figure 3. Exoskeletal structure of HAL-3.

around the knee joint were carried out, so the angle of the knee joint, the force applied by the operator's lower thigh, and the myoelectricity at the biceps femoris as flexor muscle and vastus medialis as extensor muscle of the knee joint were measured as the required data for the evaluation of the experimental results. The measured data were fed to the control computer at a sampling rate of 1 kHz.

2.2. Identification of dynamic parameters of the exoskeleton of HAL-3

The dynamic parameters of HAL-3's exoskeleton, such as inertia moment, viscous friction coefficient, gravitational moment and Coulomb friction, were identified before the experiments in order to adjust the virtual impedance. The motion equation around the knee joint of the exoskeleton is expressed as (1):

$$I_h \frac{d^2\theta(t)}{dt^2} + D_h \frac{d\theta(t)}{dt} + M_h g l_h \sin\theta(t) + C_a \operatorname{sign}\left(\frac{d\theta(t)}{dt}\right) = \tau_a(t), \qquad (1)$$

where I_h, D_h, $M_h g l_h$ and C_a represent inertia moment, viscous friction coefficient, gravitational moment and Coulomb friction around the knee joint of the exoskeleton, respectively, $\theta(t)$ is the angle of the knee joint, $\operatorname{sign}(d\theta(t)/dt)$ is the sign of the angular velocity, and $\tau_a(t)$ is the torque generated by the actuator. Equation (1) can be expressed by:

$$\Omega(t)X = \tau_a(t), \qquad (2)$$

where:

$$\Omega(t) = \left[\frac{\mathrm{d}^2\theta(t)}{\mathrm{d}t^2}\frac{\mathrm{d}\theta(t)}{\mathrm{d}t}\sin\theta(t)\,\mathrm{sign}\left(\frac{\mathrm{d}\theta(t)}{\mathrm{d}t}\right)\right], \tag{3}$$

$$X = [I_\mathrm{h}\ \ D_\mathrm{h}\ \ M_\mathrm{h}gl_\mathrm{h}\ \ C_\mathrm{a}]^\mathrm{T}. \tag{4}$$

When $\hat{X}(t)$ and ε represent the matrix of unknown parameters to be identified and the error between estimated torque calculated with $\hat{X}(t)$ and measured torque, respectively, $\tau_\mathrm{a}(t)$ is expressed as:

$$\tau_\mathrm{a}(t) = \Omega(t)\hat{X}(t) + \varepsilon = \hat{\tau}_\mathrm{a}(t) + \varepsilon, \tag{5}$$

where $\hat{\tau}_\mathrm{a}(t)$ is estimated torque. Based on the condition to minimize the squared error ε^2 as:

$$\frac{\partial J(t)}{\partial \hat{X}(t)} = 0, \tag{6}$$

$$J(t) = \varepsilon^\mathrm{T}\varepsilon = \big(\tau_\mathrm{a}(t) - \Omega(t)\hat{X}(t)\big)^\mathrm{T}\big(\tau_\mathrm{a}(t) - \Omega(t)\hat{X}(t)\big), \tag{7}$$

unknown parameters $\hat{X}(t)$ are found as (8):

$$\hat{X}(t) = \big(\Omega(t)^\mathrm{T}\Omega(t)\big)^{-1}\big(\Omega(t)^\mathrm{T}\tau_\mathrm{a}(t)\big). \tag{8}$$

In the experiments for parameter identification, the actuator was driven in sinusoidal patterns with frequencies of 0.33, 0.67 and 1.33 Hz, which gave better experimental results in the preceding trials [7]. Angular acceleration and angular velocity were calculated from the smoothed difference values of angle data. In total, 10 experiments were performed, and parameters were found as the mean values of experimental results. Table 1 summarizes the mean values of the identified parameters of HAL-3's exoskeleton.

Table 1.
Identified parameters around the knee joint of the exoskeleton (means ± SD of 10 trials)

Parameters	Identified values
Inertia moment ($\mathrm{kg\,m^2}$)	0.17 ± 0.001
Viscous coeff. (N m/(rad/s))	3.13 ± 0.08
Gravitational moment (N m)	3.31 ± 0.004
Coulomb friction (N m)	0.57 ± 0.02

3. EXPERIMENTAL DETAILS

In this paper, the experiments were performed in two steps: (i) the virtual impedance values around the knee joint of HAL-3 were adjusted individually and (ii) the virtual impedance values were adjusted properly based on former experimental results. The relationships between the physical stress and the virtual impedance were then analyzed.

3.1. Experimental system composed of the operator and HAL-3

The equation of motion of the operator's lower thigh including the exoskeleton of HAL-3 can be expressed as:

$$(I_s + I_h)\frac{d^2\theta(t)}{dt^2} + (D_s(u(t)) + D_h)\frac{d\theta(t)}{dt} + (M_s g l_s + M_h g l_h)\sin\theta(t) + C_a \operatorname{sign}\left(\frac{d\theta(t)}{dt}\right) = \tau_a(t) + \tau_m(t), \tag{9}$$

where I_s, D_s and $M_s g l_s$ represent inertia moment, viscous friction coefficient and gravitational moment around the knee joint of the operator, respectively, $u(t)$ is the muscle activation at the knee joint of the operator, and $\tau_m(t)$ is the torque generated by the muscles (musculoskeletal moment). Note that I_h, D_h, $M_h g l_h$ and C_a are previously identified parameters (Table 1). In (9), we assumed the stiffness by the operator's muscles is very small in comparison with other parameters. When compensating torque is generated by actuator as:

$$\tau_a(t) = (I_h - I_v)\frac{d^2\theta(t)}{dt^2} + (D_h - D_v)\frac{d\theta(t)}{dt} + (M_h - M_v)g l_h \sin\theta + (C_a - C_v)\operatorname{sign}\left(\frac{d\theta(t)}{dt}\right). \tag{10}$$

Substituting $\tau_a(t)$ from (10) into (9) results in the experimental motion expressed as (11):

$$(I_s + I_v)\frac{d^2\theta(t)}{dt^2} + (D_s(u(t)) + D_v)\frac{d\theta(t)}{dt} + (M_s g l_s + M_v g l_h)\sin\theta(t) + C_v \operatorname{sign}\left(\frac{d\theta(t)}{dt}\right) = \tau_m(t), \tag{11}$$

where I_v, D_v, $M_v g l_h$ and C_v represent virtual impedance which can be chosen by the experimenter.

Figure 4 depicts the configuration of the overall experimental system. The operators were seated on a firm platform so as to be able to swing his/her lower thigh stably for a long time. An experimenter could browse the measured data such as the angle of the joint and adjust the experimental settings with a palm-top computer through a wireless LAN.

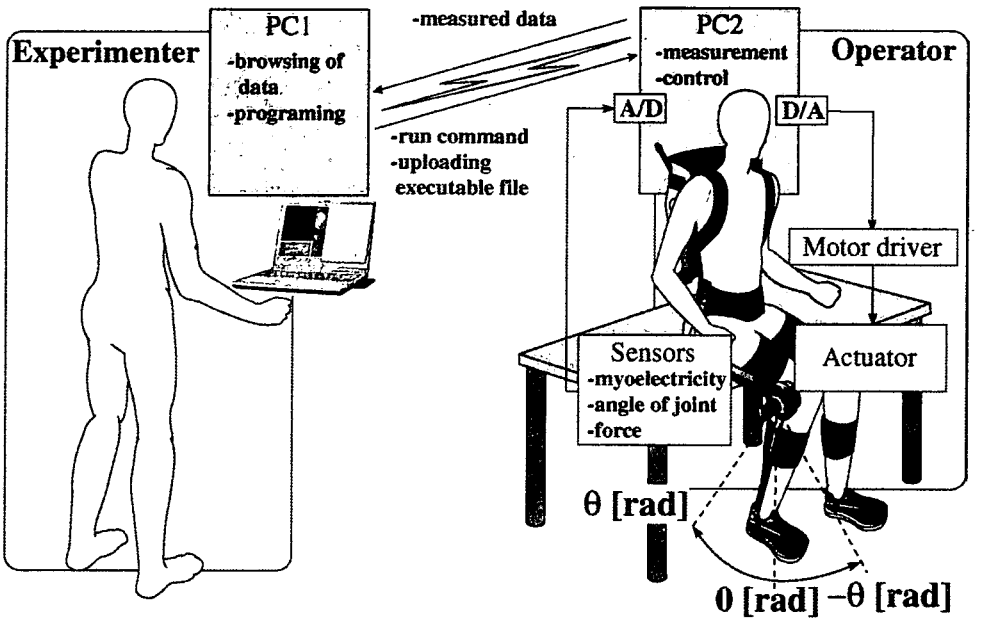

Figure 4. Schematic overview of the experimental system.

Table 2.
The set values of the virtual impedance

Virtual impedance	Set value	Tolerance
I_v (kg m^2)	0.170 to −0.020	−0.020
D_v (N m/(rad/s))	3.128 to −0.782	−0.391
$M_v g l_h$ (N m)	3.310 to −0.828	−0.414
C_v (N m)	0.560 to −0.140	−0.070

3.2. Settings of experimental condition

In the experiments, the operators were instructed to swing their lower thigh according to the same boundary values and frequency so that we could evaluate unconstrained motions under the same conditions. The boundary values of the knee joint angle and frequency for unconstrained motion were set to ±0.5 rad and 1 Hz, respectively [7]. Figure 5 depicts the myoelectricity at the flexor and extensor muscles, the musculoskeletal moment calculated based on the measured force, and the angle of the knee joint measured in the experiments.

Experiments were performed in two steps. In the first step, the virtual impedance around the knee joint of HAL-3 was adjusted individually in 10 steps as shown in Table 2. The operator swung his/her lower thigh for 10 min, and the experimental trials were performed in sets of 10 steps 5 times for an operator and for virtual impedance. In the second step, the virtual impedance was adjusted properly at once,

based on the results of the former experiments, and the operators swung his/her lower thigh as in the first experiments.

The operators were three unimpaired persons who were 28 (A), 22 (B) and 21 (C) years old, respectively. They had break times between trials so that muscular fatigue did not have an influence on the motions of the operators and the myoelectricity [8].

3.3. Method of evaluation of the experimental results

It is likely that the method of evaluation of the the experimental results should include not merely objective, but also subjective factors since the overall experimental system is composed of a robot and a human.

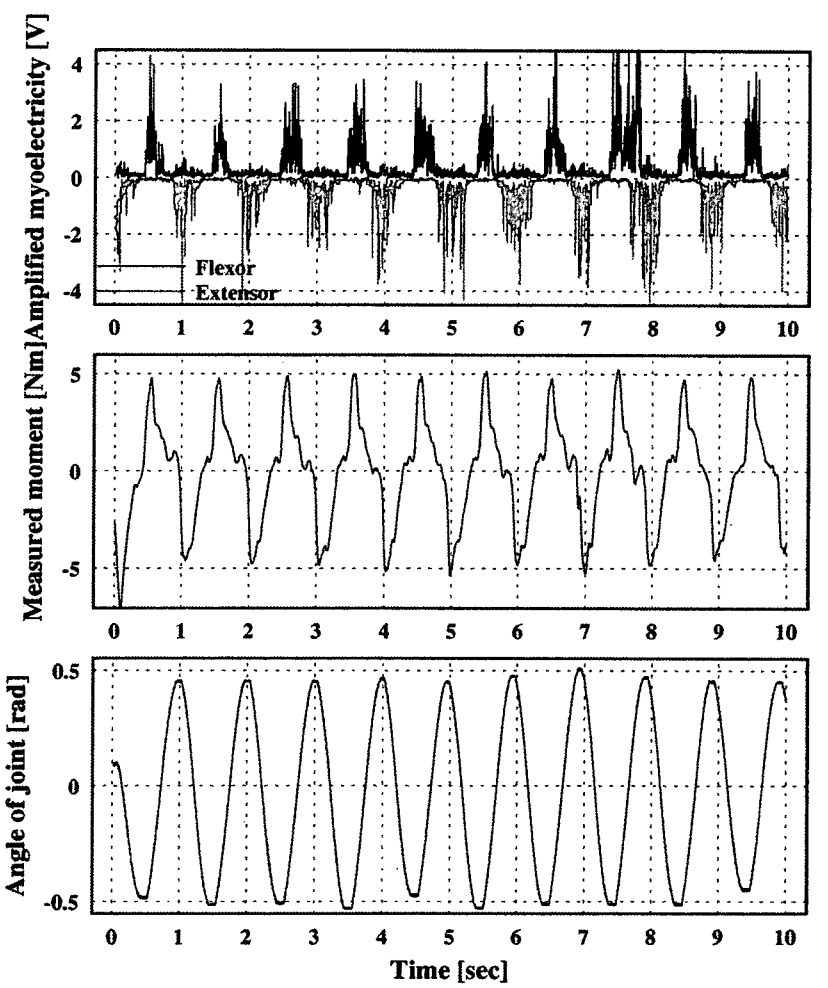

Figure 5. Data of the experimental motion (myoelectricity at the flexor and extensor muscles, musculoskeletal moment applied to exoskeleton and angle of joint).

In order to evaluate the experimental results objectively, physical stress in the experiment was evaluated with the mean value of musculoskeletal moment calculated based on the measured force as:

$$J_{\tau_m}(i) = \frac{1}{t_f}\int_0^{t_f} |\tau_m(t, i)|\, dt, \tag{12}$$

and the integral values of myoelectricity normalized with the maximum in the overall trials for estimating which muscle contributed to the experimental motion as:

$$J_{m_f}(i) = J_f(i)/J_{f_{max}}, \tag{13}$$

$$J_{m_e}(i) = J_e(i)/J_{e_{max}}, \tag{14}$$

where:

$$J_f(i) = \int_0^{t_f} |m_f(t, i)|\, dt, \tag{15}$$

$$J_e(i) = \int_0^{t_f} |m_e(t, i)|\, dt, \tag{16}$$

$$J_{f_{max}} = \max\{J_f(1), \ldots, J_f(n)\}, \tag{17}$$

$$J_{e_{max}} = \max\{J_e(1), \ldots, J_e(n)\}. \tag{18}$$

In (12)–(18), n and t_f represent number of trials for each operator and trial duration, respectively, $\tau_m(t, i)$ is the measured musculoskeletal moment, $J_{\tau_m}(i)$ is the mean value of the musculoskeletal moment, $m_f(t, i)$ and $m_e(t, i)$ are the myoelectricity values at the flexor and extensor muscle, respectively, and $J_{m_f}(i)$, $J_{m_e}(i)$ are the normalized myoelectricity values at the flexor and extensor muscle, respectively.

The Semantic Differential (SD) method was used for the evaluation of the operator's feeling as summarized in Table 3 [6, 9, 10] for the subjective evaluation of experimental results. In Table 3, operationality was defined as the feeling of whether an operator could swing the leg according to the his/her intention or not

Table 3.
Evaluation of the operator's feelings

	Mark						
	−3	−2	−1	0	1	2	3
Operationality	very bad	bad	slightly bad	—	slightly good	good	very good
Stress level	very heavy	heavy	slightly heavy	—	slightly light	light	very light

and the stress level as the feeling of 'light' or 'heavy'. As a reference for the feeling evaluated in the experiments, when the virtual impedance was not adjusted at all, the marks of the operationality and stress level were set to 2 and −3, respectively. The operators were well rehearsed so as to understand the meaning of operationality and stress level in the evaluation before the experiments. The experimental results were evaluated mainly with the musculoskeletal moment, which reflects the efficiency of motions.

4. RESULTS

4.1. Basic experiments for adjustment of virtual impedance

Figures 6–8 depict the experimental results of musculoskeletal moment and myoelectricity at the flexor and extensor muscles respectively. Panels (a)–(d) indicate the experimental data for adjustment of virtual inertia moment viscous friction, gravitational moment and Coulomb friction, respectively. The results were obtained from 220 trials for each operator, i.e., total of 660 trials.

The amount of musculoskeletal moment and myoelectricity tended to decline gradually with the decrease of the positive virtual inertia moment and virtual Coulomb friction in panels (a) and (b) of Figs 6–8.

In particular, the amount of musculoskeletal moment decreased markedly for operators A and B. In contrast, musculoskeletal moment and myoelectricity had a tendency to remain steady or increase slightly for the negative values of the virtual inertia moment and the virtual Coulomb friction, and it is likely that the negative virtual impedance made the experimental motion unstable.

In the case of the virtual gravitational moment in panel (c) of Figs 6–8, the amount of musculoskeletal moment tended to increase slightly. The changes of myoelectricity were divided depending on the operator into the case of rising slightly and the case of increasing and decreasing in turn. Hence, we could be fairly certain that the gravitational moment by exoskeleton of HAL-3 did not impede the operator's motion and it is possible that the operators could swing their lower thigh effectively by using the gravitational moment.

The results of experiments for the virtual viscous friction in panel (d) of Figs 6–8 were divided into the case of operator A, and the case of operators B and C. In the case of operator A, the amount of musculoskeletal moment and myoelectricity at the extensor muscle rose with the decrease of the virtual viscous friction, and myoelectricity at the flexor muscle changed irregularly compared to operators B and C. Thus, it is likely that operator A could not correspond properly to the change of virtual viscous friction although he tried to let the experimental motion stabilize by using the muscles. In the case of operators B and C, the decrease of virtual viscous friction made the musculoskeletal moment and the myoelectricity at the flexor increase gradually after it declined to a trough at the positive virtual viscous friction. The amounts of myoelectricity at the extensor muscles of operators A–C

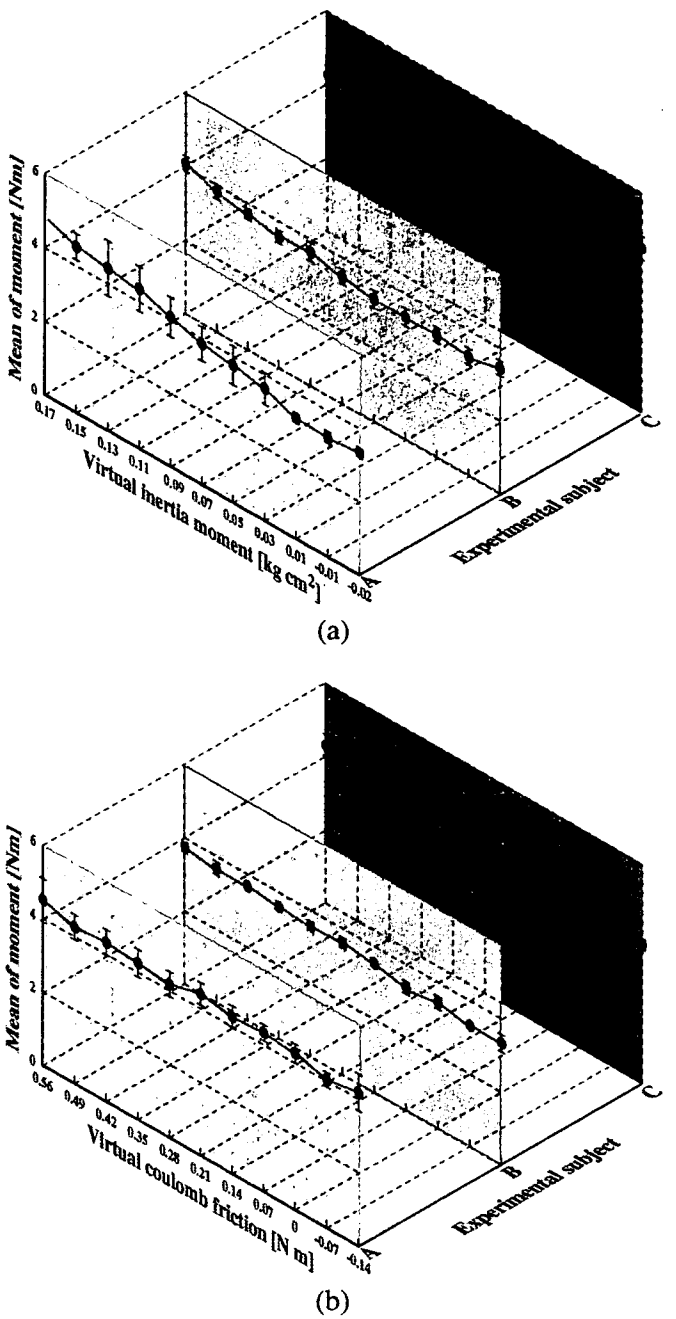

Figure 6. Experimental results for musculoskeletal moment.